SUPPLEMENTAL DATA

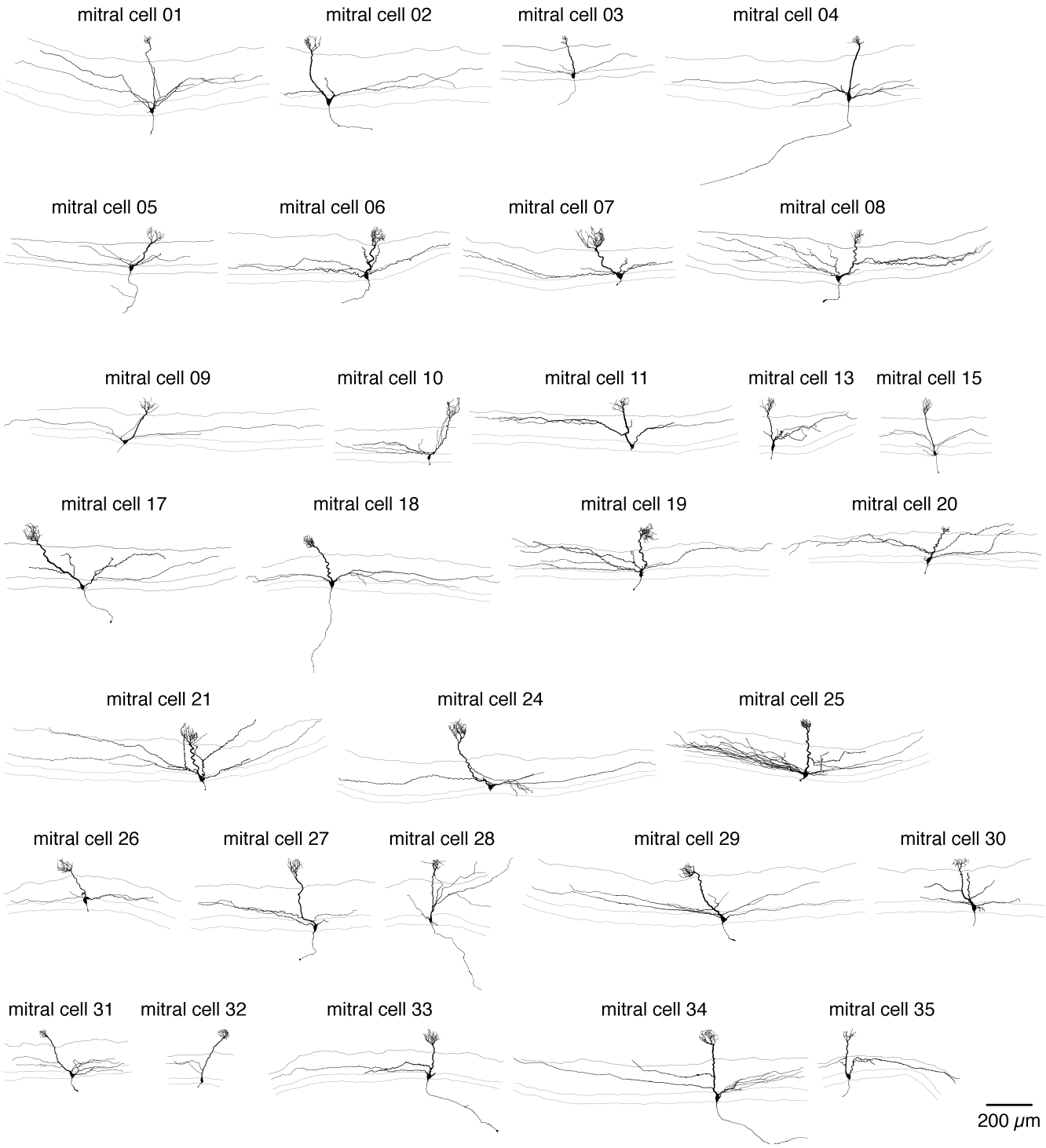

Figure S1. MC morphology. Reconstructed morphologies of 30 MCs recorded for analysis of intrinsic MC biophysical properties. The MCL is bracketed by light grey contours and the division between the GL and EPL is shown by a dark grey contour. Scaling is equivalent for Figs. S1 and S2.

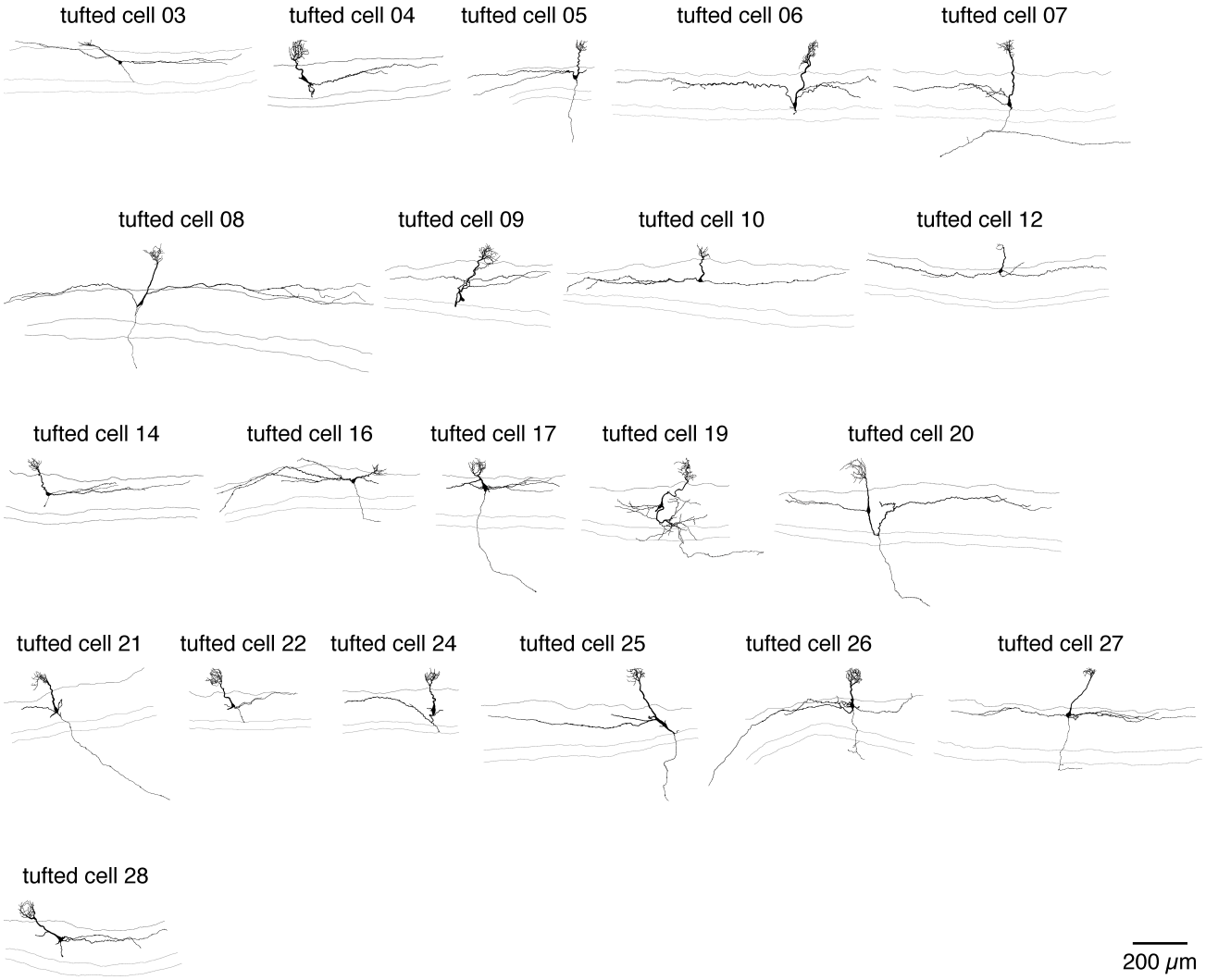

Figure S2. TC morphology. Reconstructed morphologies of 21 TCs recorded for analysis of intrinsic TC biophysical properties. The MCL is bracketed by light grey contours and the division between the GL and EPL is shown by a dark grey contour. Scaling is equivalent for Figs. S1 and S2.

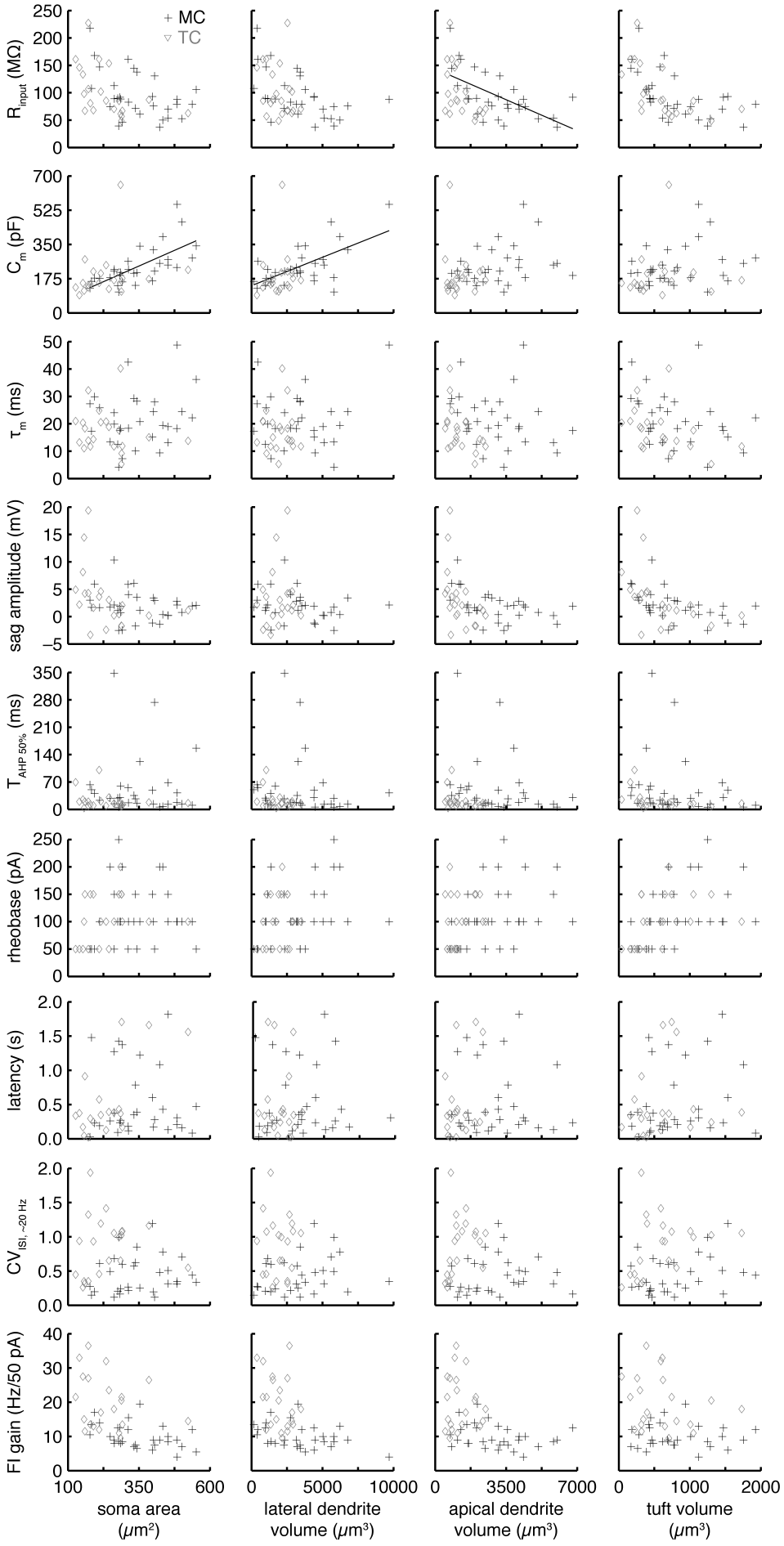

Figure S3. MC and TC intrinsic biophysical properties are largely independent of morphological properties. Linear regression analysis was performed between physiological and morphological properties for MCs (n=30) and TCs (n=21). Significant relationships (with Bonferroni correction for multiple comparisons) are plotted as black (MCs) and grey (TCs) lines. MC R_{input} significantly decreases with increasing apical, but not lateral, dendrite volume ($p=4.0\times10^{-4}$; $R^2=0.37$). In contrast, MC C_m significantly increases with increasing soma area ($p=3.5\times10^{-5}$; $R^2=0.46$) and lateral dendrite volume (1.2×10^{-4}; $R^2=0.41$). No significant relationships were observed between TC physiological and morphological properties.

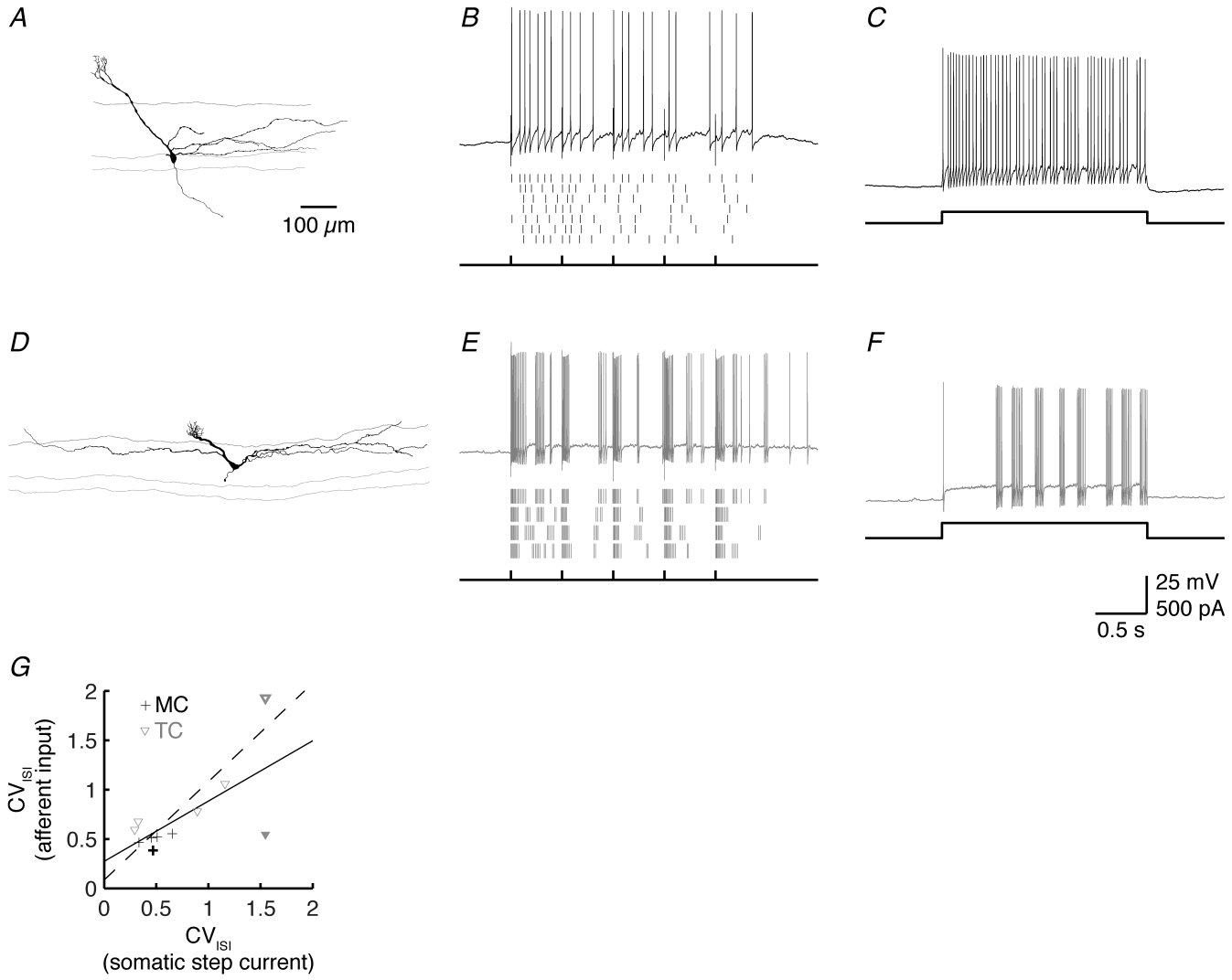

Figure S4. The diversity of afferent-evoked firing modes is predicted by somatic step current injections. ***A-C:*** Representative MOB principal neuron (A) exhibiting a regular firing response to both afferent stimulation (B) and somatic step current injection (C). Raster plots in ***B*** show the firing response across multiple successive trials of 2 Hz afferent stimulation (first row shows the example spiking response plotted at top). ***D-F:*** Same as ***A-C***, but for a MOB principal neuron exhibiting a stuttering firing response. ***G:*** CV_{ISI} of the firing response to afferent stimulation vs. the CV_{ISI} of the firing response to somatic step current injection (evoking a ~20 Hz firing rate) for 5 MCs (black crosses) and 6 TCs (grey diamonds). Thick-lined symbols correspond to the regular and stuttering neurons shown in ***A*** and ***D***, respectively. Solid grey diamond plots the firing response of a stuttering TC with long action potential clusters observed during somatic step current injections. These long action potential clusters generated regular patterns of action potentials within the relatively shorter afferent stimulation cycles, thus yielding a high somatic step current-evoked CV_{ISI} and a low afferent evoked CV_{ISI}. Including this outlier, the CV_{ISI} evoked by somatic step current injection significantly predicted the CV_{ISI} evoked by afferent input (solid line; linear regression: $p=0.03$; $R^2=0.44$). Omission of the outlier revealed a more robust relationship (dashed line; linear regression: $p=3.5\times10^{-4}$; $R^2=0.81$).

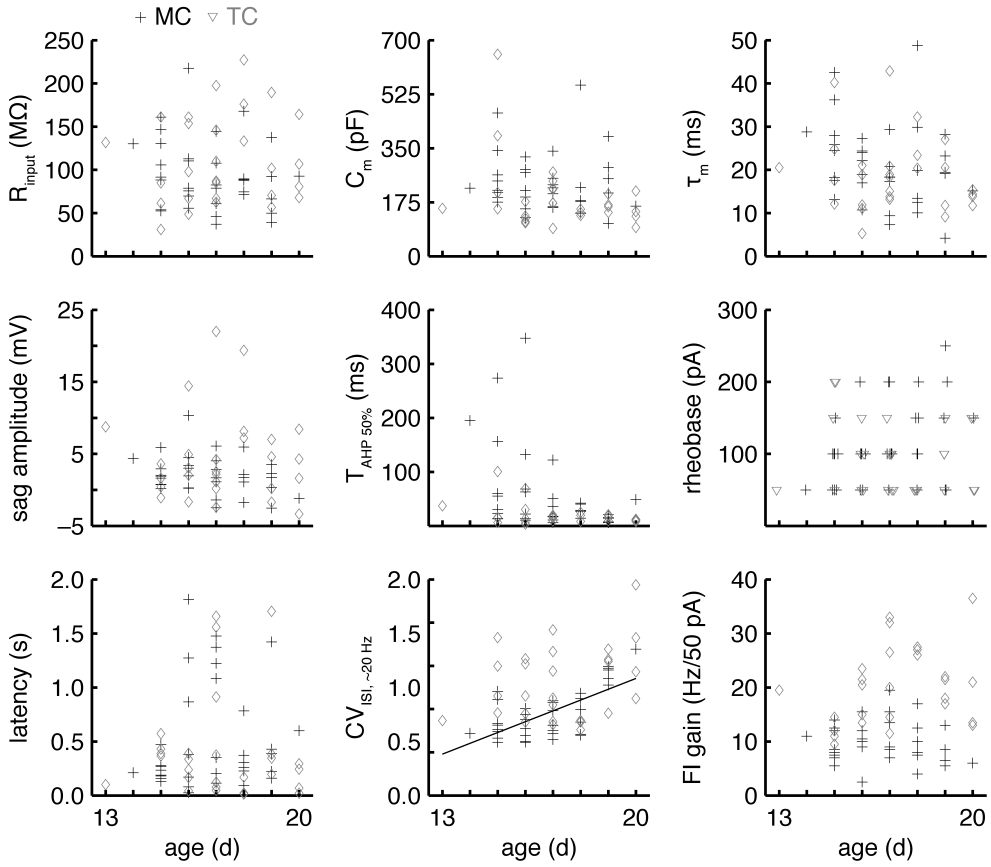

Figure S5. Biophysical diversity within MCs and TCs is largely independent of age. Linear regression analysis was performed between animal age and R_{inpu}, C_m, τ_m, sag amplitude, $T_{AHP\ 50\%}$, rheobase, first spike latency at rheobase, $CV_{ISI,\ \sim 20\ Hz}$, and FI curve gain for MCs and TCs. Significant relationships (with Bonferroni correction for multiple comparisons) are plotted as black (MCs) and grey (TCs) lines. Age values have been jittered by ~0.1 d in the plot of rheobase vs. age to help visualize overlapping data points. MC firing regularity significantly decreases with animal age ($p=1.2\times10^{-5}$; $R^2=0.44$). Variance in other MC and TC biophysical properties could not be explained by age differences.

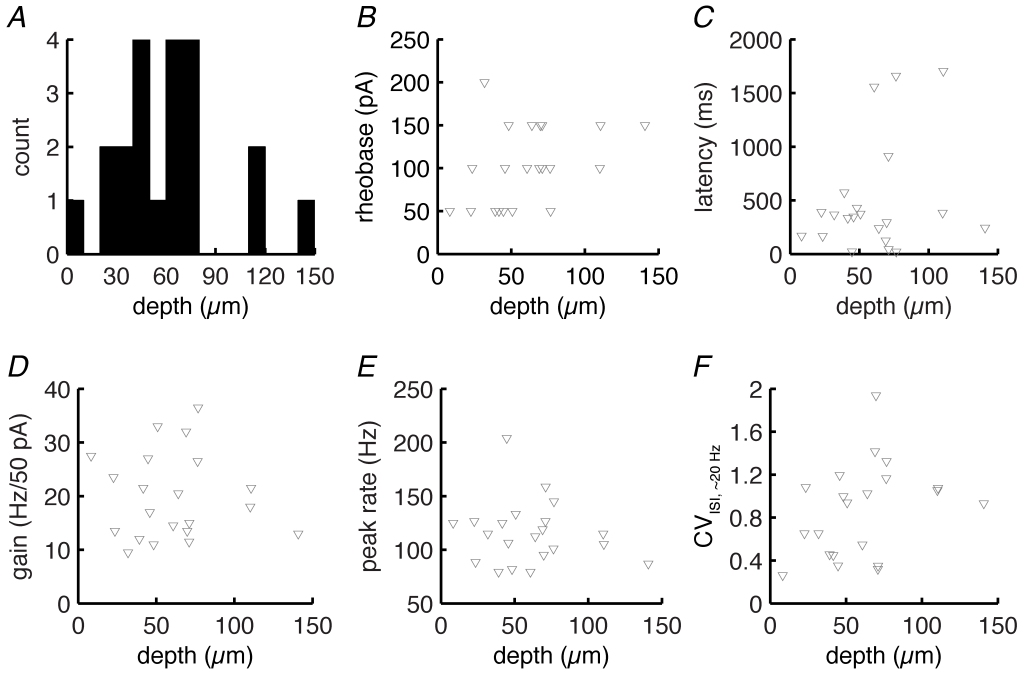

Figure S6. Depth analysis of TCs. ***A:*** Distribution of somatic depths from the GL-EPL border of reconstructed TCs (see Fig. S2 for full reconstructions). ***B-F:*** Linear regression of somatic depth against rheobase (B; p=0.09), first spike latency at rheobase (C; p=0.24), FI curve gain (D; p=0.84), peak instantaneous firing rate (E; p=0.56), CV_{ISI} measured at ~20 Hz (F; p=0.12).